J. Fluid Mech. (2001), *vol.* 449, *pp.* 201–224.
DOI: 10.1017/S0022112001006292 Printed in the United Kingdom

The transition from inertia- to bottom-drag-dominated motion of turbulent gravity currents

By ANDREW J. HOGG[1] AND ANDREW W. WOODS[2]

[1]Centre for Environmental and Geophysical Flows, School of Mathematics, University of Bristol, University Walk, Bristol BS8 1TW, UK

[2]BP Institute, University of Cambridge, Madingley Rise, Cambridge CB3 0EZ, UK

(Received 13 February 2001 and in revised form 5 July 2001)

The influence of drag on the motion of gravity currents over rigid horizontal surfaces is considered analytically using a Chézy model of boundary shear stress. Although the initial motion is governed by a balance between the buoyancy forces and fluid inertia, drag gradually influences the flow. The length and time scales at which these effects become significant are identified. A perturbation series, valid at early times, is constructed to analyse the changes to the velocity and height of the evolving current due to drag. At much later times, a new class of similarity solutions is developed to model the motion which is now governed by a balance between buoyancy and drag. The transition in the dominant forces which govern the dynamics of the flow is examined by numerically integrating the equations of motion for flows generated by a constant flux of relatively dense fluid. The numerical results confirm both the perturbation solution, valid at early times, and the new similarity solution valid at late times. The transition between the two may involve the formation of a discontinuity (bore). Finally particle-driven currents, which exhibit different dynamical behaviour due to the progressive reduction of their density arising from particle sedimentation, are investigated.

1. Introduction

Gravity currents are common in nature and in many industrial applications. They occur when a fluid intrudes into another of a different density, resulting in a buoyancy-driven flow. For example, when a fluid is introduced into a less dense ambient, a gravity current arises and the fluid spreads along the underlying boundary. Such flows may arise when a relatively heavy pollutant is discharged into a river or estuary or when there is a release of a dense gas in the atmosphere. In both of these situations the difference in the densities of the two fluids is due to compositional differences. Alternatively, the excess density of the intruding fluid may arise as a result of the suspension of relatively heavy particles. In this case the dynamics of the gravity current are more complicated because the particles settle out of the suspension and thus the initial density difference is progressively reduced. Examples of these flows include turbidity currents in the oceans and volcanic pyroclastic flows. The properties of gravity currents and their importance in many other applications have been discussed by Simpson (1997).

The purpose of this study is to consider the effects of drag upon the motion of

gravity currents. Viscous gravity currents have been studied by Huppert (1982), in which the resistive force is proportional to the viscous stress exerted by the underlying boundary. High-Reynolds-number flows over horizontal boundaries have usually been assumed to be unaffected by drag because the inertial forces far exceed the viscous forces. In this study, however, we consider the effect on the propagation of gravity currents of the drag associated with turbulent fluid motions. In its simplest form, this stress per unit mass may be modelled by a constant drag coefficient multiplied by the square of the speed of the overlying flow (Moody 1944; Turner 1973). Such a Chézy model of drag has been employed widely in studies of channel flow over rough boundaries composed of bed topography of low aspect ratio as well as in studies of estuarine salt wedge formation and the flow of gravity currents down slopes (Turner 1973).

For many cases the influence of viscosity is negligible and a balance of inertial, gravitational and drag forces dominates the dynamics of the flow. Furthermore, the horizontal lengthscale of the motion usually far exceeds the vertical. Therefore the pressure distribution is hydrostatic in the vertical and the shallow-water equations may be employed to model its evolution (e.g. Whitham 1973). A boundary condition at the front of the current is added to the governing equations. For an ideal fluid, Benjamin (1968) found that when the depth of the current is much less than the depth of the ambient fluid, the Froude number at the front is equal to $\sqrt{2}$. In this context, the Froude number represents the ratio of the speed of propagation to the local speed of internal waves of long wavelength. Huppert & Simpson (1980) studied this condition experimentally and found the ratio to be 1.19. They attributed the difference to unsteady and three-dimensional motions around the front of the gravity current.

The system of equations admits self-similar solutions in the absence of basal drag. These solutions are useful because they provide intermediate asymptotics for the flow. They are valid for intermediate times when the flow is no longer strongly influenced by the initial conditions and yet the effects of friction are still negligible. The solutions have been classified by Grundy & Rottman (1986) and Gratton & Vigo (1994). Four types of solution emerge which depend on the conditions at the front and the source: continuous; continuous with supercritical–subcritical transitions; discontinuous with hydraulic jumps; and discontinuous with two hydraulic jumps and a supercritical–subcritical transition. We note that in the context of discontinuities between two superimposed fluids, hydraulic jumps are termed internal jumps (Yih & Guha 1955).

In § 2, we review the governing equations of the flow, indicate the forms of self-similar solutions in the absence of drag and summarize the particular solutions for planar currents generated by the input of a constant flux of dense fluid (Gratton & Vigo 1994). In § 3 we calculate the short-time perturbation to the similarity solution by the inclusion of a relatively weak drag force. We then consider the long-time balance in which the drag forces dominate the inertial and balance the streamwise hydrostatic pressure gradient (§ 4). In this regime we find that the rate of propagation of the current has a different power-law dependence on time and we construct new solutions to the model. We present results of a numerical integration of the equations of motion in § 5 which illustrate the way in which this new class of solutions is established. In § 6 we investigate the difference in the dynamics of the flow when the excess density is generated by the suspension of particles which progressively sediment to the boundary, thus reducing the difference in density between the current and the ambient fluid. Finally, in § 7, we summarize the results and illustrate some applications of this work.

2. Governing equations

We consider the motion of a gravity current in which a fluid of density ρ_c intrudes along a horizontal boundary beneath a lighter ambient fluid of density ρ_a. The horizontal lengthscale of the flow is assumed to be much greater than the vertical lengthscale. Vertical accelerations are neglected and the pressure is hydrostatic (see, for example, Whitham 1973). This implies that the shallow-water equations may be employed and the evolution of the current can be described in terms of its velocity and height, denoted by u and h, respectively. These are functions of time, t, and of a horizontal spatial coordinate, x, which is the distance from a line source in two-dimensional geometry and the radial distance from a point source in an axisymmetric geometry. In most of the analysis which follows in this study, we pursue a description of planar currents, but in this section and the Appendix we employ an analytical framework which includes axisymmetric currents.

Recent experimental studies have investigated the mixing of the relatively dense gravity current with the surrounding ambient fluid for flows over horizontal boundaries (Hallworth *et al.* 1996). Although they find there is some entrainment of the ambient, the overall rate of entrainment is low. Thus, on the assumption that the current does not entrain ambient fluid, conservation of mass is given by

$$\frac{\partial h}{\partial t} + x^{-n}\frac{\partial}{\partial x}(x^n u h) = 0, \tag{2.1}$$

where $n = 0$ and $n = 1$ for planar and axisymmetric flows, respectively. On the assumption that the density difference between the ambient fluid and the gravity current is small so that the Boussinesq approximation may be made, the vertically integrated momentum equation is given by

$$\frac{\partial}{\partial t}(uh) + x^{-n}\frac{\partial}{\partial x}(x^n u^2 h) + \frac{\partial}{\partial x}(\tfrac{1}{2}g' h^2) = -\tau_b/\rho_c, \tag{2.2}$$

where τ_b is the basal shear stress exerted on the lower boundary and $g' \equiv (\rho_c - \rho_a)g/\rho_a$ is the reduced gravity. If viscous forces were non-negligible and the fluid were Newtonian, then this stress could be related to the product of the strain rate and the dynamic viscosity. Viscously dominated flows have been studied by Huppert (1982). However, in this study, we are interested in the effect of turbulent stresses. We therefore introduce a drag coefficient, C_D, which will be assumed constant, to relate the shear stress to the mean flow speed,

$$\tau_b = \rho_c C_D u^2. \tag{2.3}$$

Typical values of the drag coefficient are in the range 0.01–0.001 (Moody 1944), depending on the roughness of the boundary. The gravity current is assumed to be non-entraining and the source of the fluid is such that the total volume is given by

$$\int_0^{x_N} x^n h \, \mathrm{d}x = q t^\alpha, \tag{2.4}$$

where $x_N(t)$ is the position of the front of the current. Note the important cases $\alpha = 0$ and $\alpha = 1$, corresponding to constant-volume and constant-flux releases of fluid. Following Benjamin (1968) and Huppert & Simpson (1980), we assume that the Froude number at the front of the current is constant

$$\frac{u}{(g'h)^{1/2}} = Fr \quad \text{at} \quad x = x_N(t). \tag{2.5}$$

Also, we assume that the source Froude number, F_0, is known,

$$\frac{u}{(g'h)^{1/2}} = F_0 \quad \text{at} \quad x = 0. \tag{2.6}$$

The specification of this condition permits the difference between sub- and supercritical conditions at the source to be analysed (Gratton & Vigo 1994).

This system of equations admits the possibility of discontinuous solutions. Supposing that a discontinuity were propagating at speed c and were at a position $x = x_s(t)$, then the matching conditions across it are given by (Whitham 1973)

$$[h(u-c)]_{x=x_s-}^{x=x_s+} = 0, \tag{2.7}$$

$$[h(u-c)^2 + \tfrac{1}{2}h^2]_{x=x_s-}^{x=x_s+} = 0. \tag{2.8}$$

These jump conditions represent the conservation of mass and momentum, respectively, and are formulated on the assumption that the motion of the ambient fluid may be neglected. (If the motion of the ambient is not negligible then the jump conditions must be amended to account for the acceleration of fluid around the discontinuity, but this falls outside of the scope of this study.)

We introduce dimensionless variables by scaling lengths with respect to $(q^2 g'^{-\alpha})^{1/(2n+4-\alpha)}$ and times with respect to $(qg'^{-(n+2)})^{1/(2n+4-\alpha)}$. This leaves C_D, Fr and F_0 as the residual dimensionless parameters in the problem. Unless stated to the contrary, we hereinafter assume that h, u and x_N are dimensionless functions of the dimensionless variables x and t.

2.1. *Similarity solutions when* $C_D = 0$

In the limit of vanishing drag, the system of equations (2.1)–(2.8) admits similarity solutions (e.g. Hoult 1972; Grundy & Rottman 1986; Gratton & Vigo 1994). In general, these are given by

$$x_N = t^{(2+\alpha)/(n+3)} X_0, \tag{2.9}$$

$$u = t^{(\alpha-n-1)/(n+3)} U(y), \tag{2.10}$$

$$h = t^{2(\alpha-n-1)/(n+3)} H(y), \tag{2.11}$$

$$c = t^{(\alpha-n-1)/(n+3)} C_0, \tag{2.12}$$

where the similarity variable is $y = x/x_N$ and C_0 and X_0 are constants. The functions $U(y)$ and $H(y)$ are determined by substitution into the governing equations and the resulting ordinary differential equations are solved subject to the boundary conditions (2.4)–(2.6).

We may assess the domain of validity of these solutions by estimating the magnitude of the viscous and turbulent drag forces, relative to the inertia of the flow. In terms of dimensional variables, these forces per unit mass are denoted by F_v, F_d and F_i, respectively, and are given by

$$F_i \sim \rho_c u^2/x_N, \quad F_v \sim \mu u/h^2, \quad F_d \sim \rho_c C_D u^2/h. \tag{2.13}$$

Viscous forces may be neglected if $F_i \gg F_v$, which implies that

$$Re\, t^{(4\alpha-5n-7)/(n+3)} \gg 1, \tag{2.14}$$

where $Re = \rho_c g'^{(n+2-2\alpha)/(2n+4-\alpha)} q^{3/(2n+4-\alpha)}/\mu$ is the initial Reynolds number of the flow (Huppert 1982). Similarly, the effects of turbulent drag may be neglected if $F_i \gg F_d$,

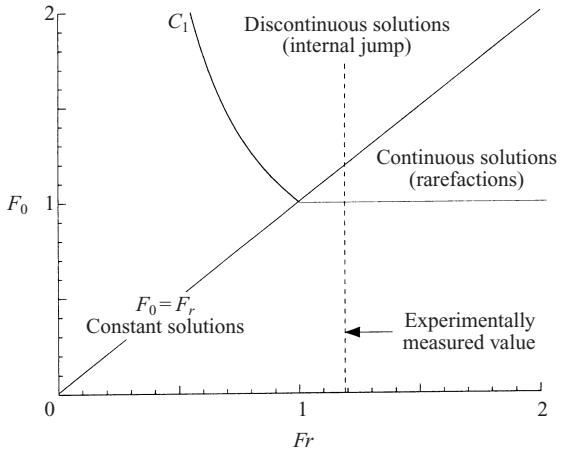

FIGURE 1. Classification of the different types of similarity solution for a planar, constant flux gravity current, determined by the Froude numbers at the source and at the front of the current. (After Gratton & Vigo 1994.)

which likewise implies that

$$C_D^{-1}\, t^{(\alpha-2n-4)/(n+3)} \gg 1. \tag{2.15}$$

This condition illustrates that, for $\alpha < 7+3n$, if the viscosity is vanishingly small, then the flow is eventually affected by the action of turbulent drag so that the buoyancy–inertial balance ceases to hold. In the course of this study, we investigate this regime and consider how turbulent drag modifies the dynamics of the flow.

2.2. *Similarity solutions for planar, constant flux gravity currents*

We now summarize the results of Gratton & Vigo (1994) for a drag-free, planar, constant flux current ($\alpha = 1, n = 0$). In this case, the scalings of the similarity solutions are particularly simple and the equations for the continuity of mass and momentum reduce to

$$-yH' + (UH)' = 0, \tag{2.16}$$

$$-yU' + UU' + H' = 0, \tag{2.17}$$

where a prime denotes differentiation with respect to y. These equations yield

$$((U-y)^2 - H)H' = 0. \tag{2.18}$$

The general solutions of the these coupled equations are

$$H = A, \quad U = B, \tag{2.19}$$

$$H = (D - \tfrac{1}{3}y)^2, \quad U = D + \tfrac{2}{3}y, \tag{2.20}$$

where A, B and D are constants. Furthermore, since (2.18) is singular at $y = U \pm \sqrt{H}$, there may be discontinuities in the derivative of H. There is also the possibility of discontinuous solutions in which case the solutions on either side of the discontinuity are matched together via the jump conditions (2.7) and (2.8). The form of the similarity solution is determined by the Froude numbers at the source and at the front of the current.

There are three classes of solution, as described by Gratton & Vigo (1994) and as summarized in figure 1. These include constant solutions, continuous solutions

(rarefactions) and discontinuous solutions (internal jumps). There are also regions of the (Fr, F_0)-plane for which it is not possible to construct similarity solutions, while imposing Froude numbers at both the source and the front. When the Froude numbers at the source and front are equal ($F_0 = Fr$), then the velocity and height are constant along the length of the current. If the Froude number at the front is supercritical and exceeds that at the source ($Fr > F_0 > 1$), then the velocity of the flow increases towards the front, whilst the height of the current decreases. The solutions are continuous but there are internal points of transition beyond which the velocity increases linearly and the height decreases quadratically (cf. a rarefaction wave in gas dynamics). This class of solution includes the dam-break solution, for which $F_0 = 1$ and $Fr \to \infty$ (see Whitham 1973). We note that it is not possible to construct similarity solutions of this form when $F_0 < 1$. Finally, if the Froude number at the source is greater than the Froude number at the front of the current, then there is a discontinuous solution in which two regions of constant velocity and height are joined by a moving internal jump. The velocity of this jump is determined by the matching conditions (2.7) and (2.8). The requirement that this jump is forward propagating, $c \geqslant 0$, corresponds to a minimum Froude number at the front for a given Froude number at the source. In figure 1, this requirement corresponds to the curve $\mathscr{C}_1$, which is given by

$$Fr = F_0 \left(\frac{2}{(1 + 8F_0^2)^{1/2} - 1} \right)^{3/2}. \tag{2.21}$$

If this jump is not forward propagating, then the flow undergoes a hydraulic jump at its source so that the flow immediately adjusts to the Froude number at the nose of the current. Note that only jumps from supercritical to subcritical conditions may occur since energy is dissipated over the transition (see, for example, Whitham 1973). A range of different solutions is given in figures 2(a) and 2(b). Note further that for a subcritical source, a similarity solution is only possible if the Froude numbers at the source and the front are identical and even then the propagation of waves upstream is still feasible which could alter the conditions at the source.

It is anticipated from the theoretical study of Benjamin (1968) and the experimental work of Huppert & Simpson (1980) that the Froude number at the front of the current is supercritical. (Huppert & Simpson 1980 find $Fr = 1.19$.) In this case, it is possible to construct similarity solutions which are constant, continuous or discontinuous, depending on the precise conditions at the source. We note that this classification is based upon an assumption that there is no entrainment of fluid into the moving current of relatively dense fluid. For flows with $F_0 \gg 1$, however, it is likely that entrainment is significant within the regions where the flow undergoes a hydraulic jump (Wilkinson & Wood 1971; Sherman, Imberger & Corcas 1978).

3. The effect of drag at early times

We now calculate the effects of drag on the propagation of gravity currents by means of an asymptotic expansion. This analytical approach yields a valid expansion for times $t \ll C_D^{(n+3)/(\alpha-2n-4)}$. We explore the long-time solution in § 4. We illustrate the use of this series expansion for the case of a planar, constant flux current ($n = 0,\ \alpha = 1$). The series is expanded in terms of $C_D t$, which is assumed to be much less than unity and the leading term of the expansion corresponds to the appropriate drag-free similarity solution of § 2.2. This technique for the construction

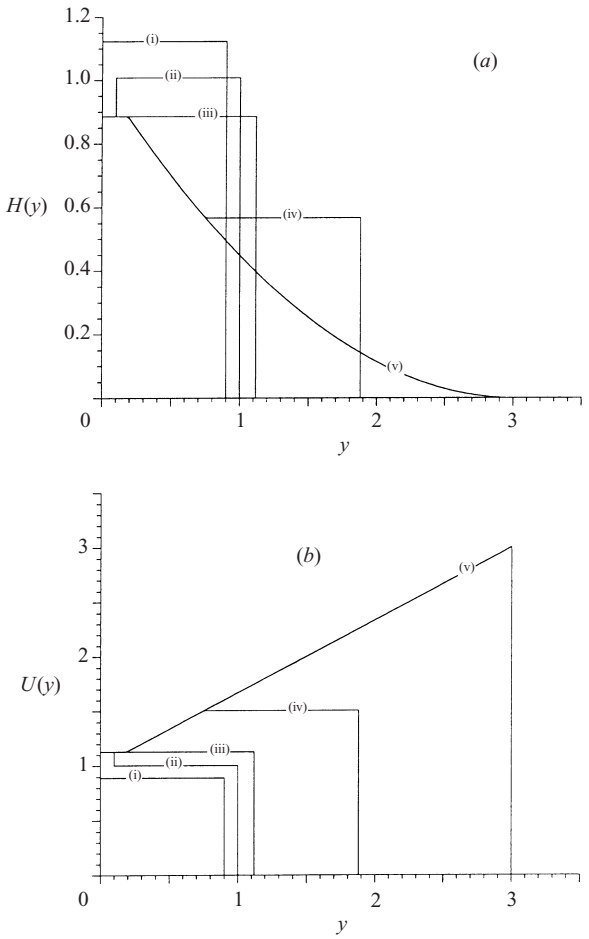

FIGURE 2. The similarity profiles of (*a*) height and (*b*) velocity for a planar, constant flux gravity current. The different solutions correspond to $F_0 = 1.2$ and (i) $Fr = 0.84$; (ii) 1.1; (iii) 1.2; (iv) 2; and (v) ∞. The first of these has a stationary internal jump at the source and is the smallest Fr for which a similarity solution exists, given $F_0 = 1.2$.

of a perturbation to an exact similarity solution has been employed recently by Hogg, Ungarish & Huppert (2000) in the examination of a particle-driven gravity current. Also Whitham (1955) and Dressler (1952) employed a somewhat similar approach to examine the effects of hydraulic resistance on dam-break flows. We pose the following series for the velocity, height and length of the current

$$x_N = X_0 t + C_D t^2 X_1 + \cdots, \tag{3.1}$$

$$u = U_0(y) + C_D t U_1(y) + \cdots, \tag{3.2}$$

$$h = H_0(y) + C_D t H_1(y) + \cdots, \tag{3.3}$$

where $y = x/(X_0 t)$. As discussed above, there may be one or more discontinuities (internal jumps) within the flow, for which series expansions for their velocities should be posed as well. In the following analysis, for simplicity, we assume that the source and frontal Froude numbers are identical ($Fr = F_0$). This implies that the

leading-order similarity solutions are continuous and given by

$$U_0 = Fr^{2/3}, \quad H_0 = Fr^{-2/3}, \quad X_0 = Fr^{2/3}. \tag{3.4a,b,c}$$

The analytical procedure described below may be equally well applied to the other classes of similarity solutions. We substitute the series into the governing equations and balance the terms at each order of C_D. The leading-order equations are automatically satisfied whereas at $O(C_D)$ we find that the equations for the conservation of mass and momentum are given by

$$H_1 - yH_1' + Fr^{-4/3}\,U_1' + H_1' = 0, \tag{3.5}$$

$$U_1 - yU_1' + U_1' + Fr^{-2/3}H_1' = -Fr^2. \tag{3.6}$$

The boundary conditions are also expanded in terms of these series. At the origin, we find that

$$U_1(0) = 0, \quad H_1(0) = 0. \tag{3.7}$$

At the nose of the current, there is a kinematic condition which yields

$$2X_1 = U_1(1). \tag{3.8}$$

On the assumption that the effects of drag are sufficiently weak that the Froude number condition still applies, we find that

$$U_1(1) = \tfrac{1}{2}Fr^{4/3}H_1(1). \tag{3.9}$$

These conditions, together with the expression for the conservation of mass (3.5), imply that the global mass balance (2.4) is automatically satisfied at $O(C_D)$. The governing equations lead to the following expression for the first-order perturbation of the height,

$$((y-1)^2 - 1/Fr^2)\frac{\mathrm{d}^2H_1}{\mathrm{d}y^2} = 0. \tag{3.10}$$

Hence, the height and velocity fields are linear functions of the similarity variable, y, and are given by

$$H_1(y) = Ay + B, \quad U_1(y) = -Fr^{4/3}(A+B)y - Fr^2 - Fr^{-2/3}A + Fr^{4/3}(A+B), \tag{3.11}$$

where A and B are constants. Furthermore, we expect a possible transition in the solution at $y = y_1 \equiv 1 - 1/Fr$, because (3.10) is singular at that point. For the experimentally determined value $Fr = 1.19$, we deduce that $y_1 > 0$.

We find that the first-order perturbations to the similarity solution are piecewise linear and are given by

$$H_1(y) = \frac{Fr^{8/3}}{Fr^2-1}y, \quad U_1(y) = -\frac{Fr^4}{Fr^2-1}y \quad \text{for} \quad 0 < y < y_1, \tag{3.12a}$$

$$H_1(y) = -\frac{Fr^{8/3}((3Fr+2)y - 3Fr)}{Fr^2+3Fr+2}, \quad U_1(y) = \frac{Fr^4(2y-3)}{Fr^2+3Fr+2} \quad \text{for} \quad y_1 < y < 1. \tag{3.12b}$$

These are plotted in figure 3. The leading-order correction to length of the current, X_1, is given by

$$X_1 = -Fr^4/[2(Fr^2+3Fr+2)], \tag{3.13}$$

which implies that, irrespective of the internal dynamics of the current, the action of drag is always to reduce the rate at which its length increases. With these solutions,

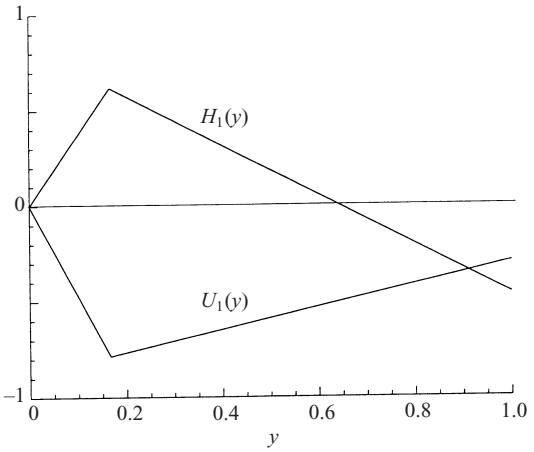

FIGURE 3. The short-time perturbation velocity and height solutions, $U_1(y)$ and $H_1(y)$, for flows with equal Froude numbers at the source and the front, given by $F_0 = Fr = 1.2$.

we now have derived the first-order correction to the drag-free similarity solution, although the solutions are only consistent for supercritical flows ($Fr > 1$). For subcritical flows, it is not possible to maintain the given source conditions and a jump occurs at the origin. (In terms of the analysis developed here, this conclusion is equivalent to the requirement that $y_1 > 0$.) We observe that for $y < y_1$, the perturbation is steady; neither the height nor velocity exhibit any explicit dependence on time. However, for $y > y_1$, the flow is unsteady. The character of the supercritical flows is that, near to the source, the velocity is reduced by the action of the drag and the height of the current increases. This implies that the local Froude number of the flow is decreasing with distance from the source. However, we require the flow to attain the same Froude number at the front as at the source. Thus, there is a transition from steady to unsteady flow and the height of the current develops a streamwise gradient to produce a (positive) streamwise pressure gradient. This compensates for the effects of drag and accelerates the fluid towards the front. The condition at the front of the gravity current can be viewed as a point of hydraulic control and $y = y_1$ is a 'choked' point, although neither is fixed in space.

This perturbation expansion is formally valid only in the regime $C_D t \ll 1$. However, the form of these first-order solutions (and subsequent higher-order solutions) indicates that close to the source there is a region in which the flow is steady and spatially developing. It is decelerated by the action of drag until it attains the critical velocity ($u = 1$) at which the local Froude number is reduced to unity. This critical velocity corresponds to the minimum momentum and energy within a steady flow with a given volume flux and reduced gravity. After this point has been attained, steady flows further downstream are no longer possible. Instead, there is a 'hydraulic catastrophe' and the flow becomes time dependent. An internal jump is set up and a bore is formed which propagates upstream. This transition is discussed in more detail in § 5, where the results of the numerical integration of the governing equations are presented. Note that these numerical results seem to indicate that this short-time perturbation solution is stable. The downstream location at which critical conditions are first attained is given by

$$x_c = C_D^{-1}(-Fr^{-2/3} + \tfrac{1}{4}Fr^{-8/3} + \tfrac{3}{4}). \tag{3.14}$$

4. The effects of drag at long times

The asymptotic series of § 3 is formally valid only for early times. After sufficient time has passed, the drag force is not just a small perturbation to the flow. Rather, it is a dominant force and different solutions must be constructed for the flow to reveal the internal dynamics. We present a new class of similarity solution in which the drag force is balanced by the developing streamwise hydrostatic pressure gradient. We focus on a planar, constant flux current ($n = 0,\ \alpha = 1$), but the analysis for a more general release and axisymmetric geometry is pursued in the Appendix.

In terms of dimensional variables, the balance between the hydrostatic pressure gradient and the drag force per unit volume is given by $\rho g' h/x_N \sim \rho C_D u^2/h$. Also, the conservation of volume implies $x_N h \sim qt$, while kinematic consistency requires $u \sim x_N/t$. Therefore, we seek a solution of the form

$$x_N = C_D^{-1/5}\, t^{4/5}\, g'^{1/5}\, q^{2/5} \mathscr{X}_0, \tag{4.1}$$

$$u = \tfrac{4}{5} C_D^{-1/5}\, t^{-1/5}\, g'^{1/5}\, q^{2/5} \mathscr{X}_0\, \mathscr{U}(\xi), \tag{4.2}$$

$$h = \tfrac{4}{5} C_D^{1/5}\, t^{1/5}\, g'^{-1/5}\, q^{3/5} \mathscr{X}_0^{3/2}\, \mathscr{H}(\xi), \tag{4.3}$$

where the similarity variable is ξ, defined by $\xi = x/x_N$. In the regime $C_D t \gg 1$, the governing equations, to leading-order, are given by

$$\mathscr{H} - 4\xi \frac{\mathrm{d}\mathscr{H}}{\mathrm{d}\xi} + 4 \frac{\mathrm{d}}{\mathrm{d}\xi}(\mathscr{U}\mathscr{H}) = 0, \tag{4.4}$$

$$\frac{\mathrm{d}\mathscr{H}}{\mathrm{d}\xi} = -\frac{\mathscr{U}^2}{\mathscr{H}}. \tag{4.5}$$

There are three boundary conditions on the flow. The kinematic condition at the front of the current is given by

$$\mathscr{U}(1) = 1. \tag{4.6}$$

The global conservation of mass is given by

$$\tfrac{4}{5} \mathscr{X}_0^{5/2} \int_0^1 \mathscr{H}\, \mathrm{d}\xi = 1. \tag{4.7}$$

Finally, by substituting these solutions into the Froude number condition at the front of the current, we deduce that the condition does not apply. Rather, the leading-order boundary condition is given by

$$\mathscr{H}(1) = 0. \tag{4.8}$$

We calculate numerical solutions for $\mathscr{H}(\xi)$ and $\mathscr{U}(\xi)$ and plot their profiles in figure 4. These solutions yield $\mathscr{X}_0 = 1.089$. An approximate solution for these functions is given by expanding for $\mathscr{H}(\xi)$ and $\mathscr{U}(\xi)$ in powers of $(1-\xi)$ to yield

$$\mathscr{H}(\xi) = [2(1-\xi) + \tfrac{1}{3}(1-\xi)^2 + \tfrac{1}{90}(1-\xi)^3 + O((1-\xi)^4)]^{1/2}, \tag{4.9}$$

$$\mathscr{U}(\xi) = 1 + \tfrac{1}{6}(1-\xi) - \tfrac{1}{180}(1-\xi)^2 + O((1-\xi)^3). \tag{4.10}$$

We note that the length of the current increases in proportion to $t^{4/5}$, which is a slower rate of propagation than in the case of drag-free motion for which the length increases linearly with t. The current also adopts a 'wedge'-shaped profile in order to generate a streamwise pressure gradient which balances the drag. The transition of a

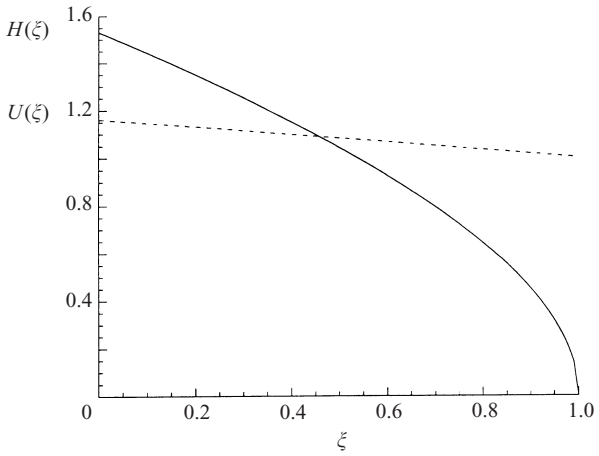

FIGURE 4. The long-time solutions for ——, height and - - - - -, velocity as functions of the similarity variable, ξ.

gravity current to a 'nose-down' mode of propagation has been noted by other studies (Simpson & Britter 1979; Ungarish & Huppert 1998; Hatcher, Hogg & Woods 2000). It reflects the fact that the current is propagating against an adverse pressure gradient or resistive force and must develop a streamwise pressure gradient, as in a viscous flow (Huppert 1982; Huppert & Woods 1995).

5. The effects of drag at intermediate times: numerical solutions

In this section, we describe the transition from the drag-free similarity solutions of § 2.2 to the drag-dependent, long-time similarity solutions of § 4. We integrate numerically the governing equations and boundary conditions described in § 2 to study the way in which the new similarity solution is approached. As before, we focus on planar, constant flux currents, although the numerical techniques may be applied equally to other geometries and source conditions. We adopt the numerical method employed by Bonnecaze, Huppert & Lister (1993). It uses a two-step Lax–Wendroff scheme, which is second-order in time and space. The computational domain is mapped into a spatial region between zero and unity by the introduction of the coordinate $\xi = x/x_N(t)$ and the equations are discretized in terms of this new variable. The boundary conditions at the source are fully specified for a constant flux current. However, the intersection of an outward propagating characteristic with the front of the current must be calculated at each time step to determine fully the boundary conditions at the front. The system of equations admits solutions with discontinuities and this scheme does not require the explicit resolution of shocks. Instead, there is implicit numerical viscosity to which a small amount of artificial viscosity is added to the momentum equation in order to damp out unphysical oscillations and maintain numerical stability. Through numerical experimentation, it is ensured that the added artificial viscosity is as small as possible in order to reproduce some of the shock-like features of the flow. Although numerical instabilities have been suppressed in most of the calculations, there is still some evidence of small oscillations around some of the discontinuities. We do not believe that these have had any significant effect on the results. The scheme is explicit in time and so a relatively small time step must be taken in order to maintain stability; however, runs times are only of the order of a

few minutes on an Ultrasparc 2200 and so this is not a problem. The total volume of the current per unit width was calculated at regular intervals by integrating the height of the current along its length and it was compared to the product of the input volume flux of fluid per unit width and the time elapsed. It was found that at all times throughout the computation, these were equal to within 0.1%, thus demonstrating that global mass conservation (2.4) is maintained.

We integrate the equations from initial conditions of $x_N = 0.2$ for three sets of parameter values. As demonstrated in §§ 3 and 4, it is the relative magnitudes of the source and frontal Froude numbers which determine the character of the solution. The magnitude of the drag coefficient, C_D, solely determines how rapidly the effects of drag are experienced. We only present results for those flows with supercritical Froude numbers at the source. Those with subcritical source conditions undergo an immediate transition in the conditions of the flow.

We first consider the evolution of the current when the Froude numbers at the source and the front are both equal to 1.2. For these values, the drag-free similarity solution of § 2.2 is that the height and velocity within the current are constant. In figures 5(a) and 5(b), we study the early time correction to this similarity solution, the analysis for which was presented in § 3. In order to do this, we evaluate the following functions

$$\delta h = \frac{h - Fr^{-2/3}}{C_D t} \equiv H_1(y) + O(C_D t), \tag{5.1}$$

$$\delta u = \frac{u - Fr^{2/3}}{C_D t} \equiv U_1(y) + O(C_D t). \tag{5.2}$$

We note that the height and the velocity fields have a piecewise linear perturbation. There is a point of transition initially located at $y = \frac{1}{6}$, as predicted in § 3. On the source-side of this point the perturbation is steady and since the source is supercritical, the velocity is progressively reduced and the height is progressively increased. In contrast, on the other side of this transitional point, the perturbation is unsteady and the height decreases and the velocity increases towards the front of the current. In figure 6, we consider the flow at later times ($C_D t = O(1)$). The general behaviour is that the flow evolves to a steady-state close to the source, while in the bulk of the current it develops a progressively increasing streamwise hydrostatic pressure gradient to balance the drag. (In figure 6 this corresponds to the time given by $C_D t = 0.125$.) This occurs until the transition point within the current is sufficiently far downstream that the velocity and height have attained critical values. (In the dimensionless units employed here this corresponds to $u = 1$ and $h = 1$.) Thereafter, the nature of the flow changes. A backward propagating bore arises from the location at which the critical conditions are first attained. This bore connects the steady near-source region to the rest of the current, in which the dynamics are beginning to become dominated by the balance between drag and the streamwise pressure gradient. The profiles of height and velocity within this region converge to the long-time similarity solution of § 4. The bore propagates backward at a relatively slow velocity. The total length of the current, x_N, exhibits a temporal increase proportional to $t^{4/5}$ well before the bore has reached the source (figure 7).

When the Froude number at the source exceeds that at the front, the drag-free similarity solution includes an internal jump which connects two regions of constant velocity and height. This jump occurs as a mechanism for the flow to dissipate energy whilst conserving mass and momentum. We study the influence of drag upon the flow when $Fr = 1.2$ and $F_0 = 2$. At early times, the perturbations to velocity and

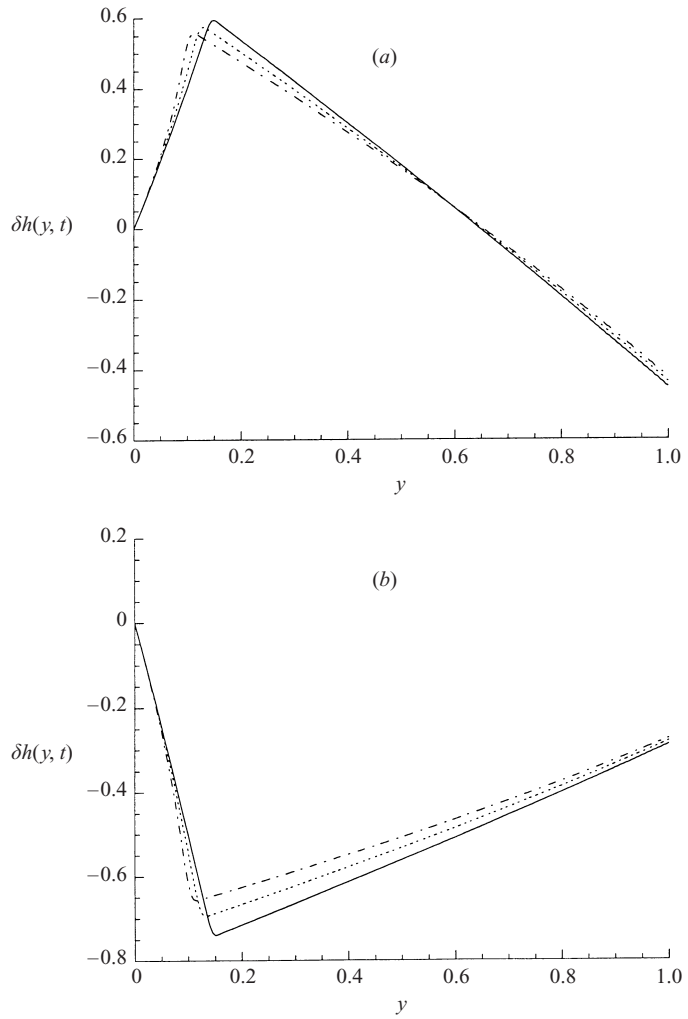

FIGURE 5. The normalized deviation of the profiles of (*a*) height and (*b*) velocity of a drag-affected gravity current from the drag-free similarity solution at short times ($C_D t \ll 1$) as functions of the similarity variable, y. In these numerical computations, $F_0 = Fr = 1.2$ and the profiles of δh and δu are shown for ——, $C_D t = 0.05$; - - - - -, 0.10; – · – · –, 0.15.

height fields are approximately linear with respect to their values in the absence of drag and the rate of propagation of the internal jump is reduced. As noted above, since the flow at the source is supercritical, the velocity is reduced and the height is increased near to the source. However, near to the front there is the opposite trend, as the current develops a streamwise hydrostatic pressure gradient. Also as noted above, the perturbation is steady on the source side of the internal transition. At later times ($C_D t = O(1)$), the internal jump has now reached the downstream location at which the flow has first attained critical conditions ($u = 1,\ h = 1$). Thereafter, an unsteady evolution occurs as the initially forward propagating internal jump reverses direction and propagates backwards and the flow evolves towards the long-time similarity solution of § 4 (figure 8). Therefore, this discontinuity propagates in both direction past a fixed downstream location between the source and the location at which critical

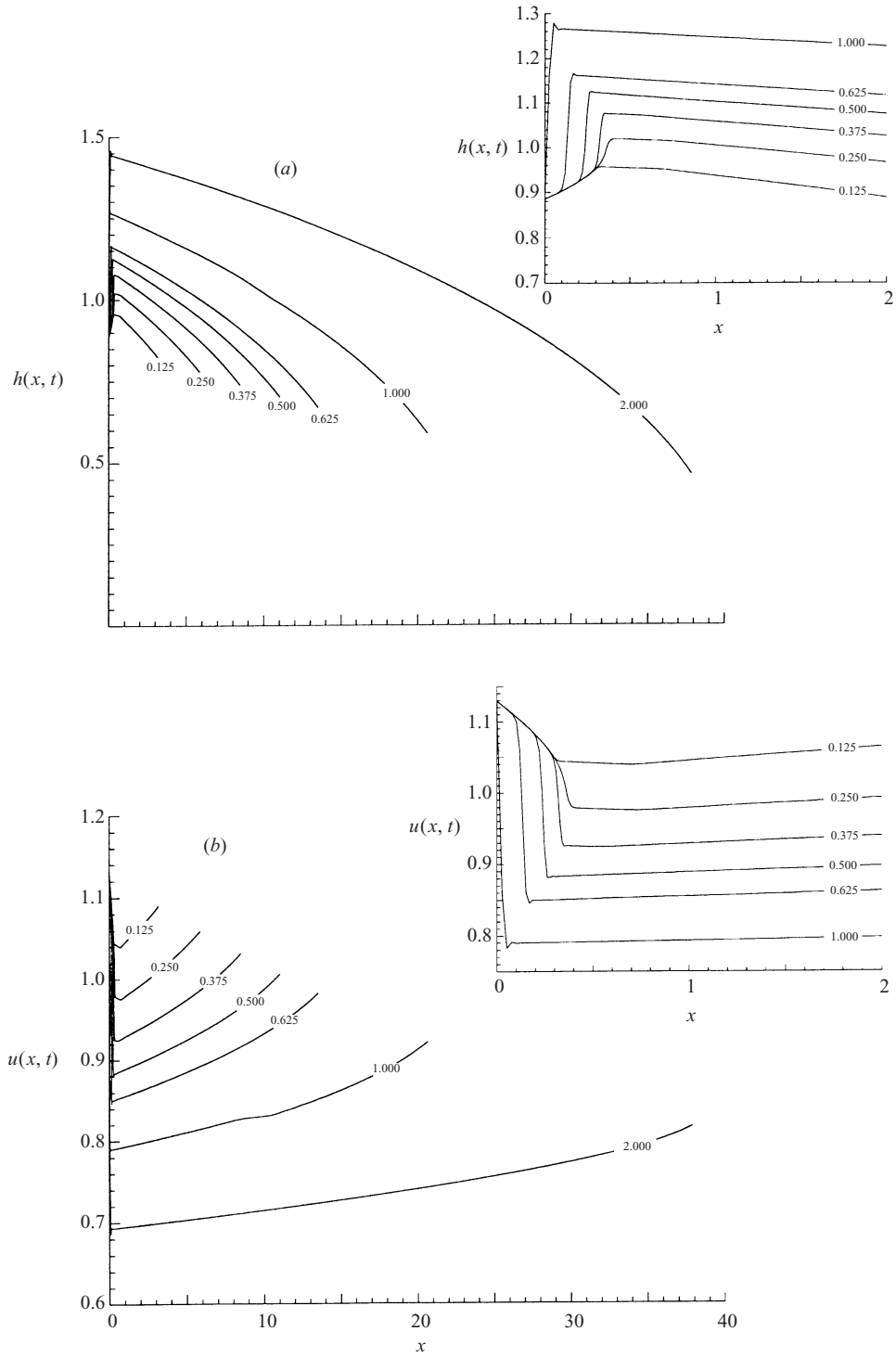

FIGURE 6. The numerically calculated profiles of (*a*) height and (*b*) velocity as functions of distance from the source at various times. These calculations were made with $Fr = F_0 = 2$ and $C_D = 0.05$. The labels on each of the profiles indicates the value of $C_D t$.

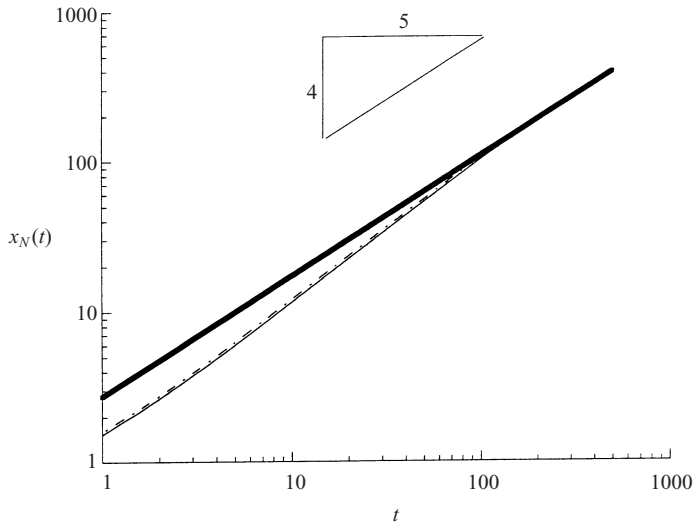

FIGURE 7. The length of the current, x_N, as a function of time. The numerical calculations were carried out with ——, $Fr = F_0 = 1.2$; - - - - -, $Fr = 1.2, F_0 = 1.15$; –·–·–, $Fr = 1.2$, $F_0 = 2$. (The first two lines are indistinguishable on these axes.) The drag coefficient, C_D, was 0.05. Note that the length of the current increases in proportion to $t^{4/5}$ in each of these cases. The bold line shows the similarity solution prediction.

conditions are first attained ($0 < x < x_c$). At early times, the internal jump propagates in the downstream direction, whereas at later times the bore propagates upstream towards the source. Once again, the length of the current grows as $t^{4/5}$ (figure 7).

The final set of numerical results is when the Froude number at the source is less than that at the front (figure 9). The drag-free similarity solution is a continuous solution in which the local Froude number within the current evolves from the value at the source to the value at the front. In this investigation, $Fr = 1.2$ and $F_0 = 1.15$ and so there are two points of transition within the current, between which the velocity varies linearly and the height quadratically and outside of which the velocity and height are constant. The effect of drag over short times is qualitatively similar to the examples above, in that near to the source the perturbation is steady, the velocity decreases and the height increases. However, the functional form of the short-time perturbation ($C_D t \ll 1$) is more complex. In the regions where the leading-order solution is constant, the perturbation is still linear, but in the region where the leading-order solution is linear in velocity and quadratic in height, the perturbation is quadratic and cubic, respectively. At later times ($C_D t = O(1)$), the dynamics of the current are very similar to those of the previous examples. The flow progressively adopts the long-time similarity solution of § 4 and a backward propagating bore is initiated from the location at which the flow first attains critical conditions. The length of the current also grows as $t^{4/5}$ (figure 7).

We have already noted that in each of these scenarios the length of the current grows as $t^{4/5}$ when $t \gg 1$. In figure 7, we also plot the similarity solution derived in § 4. This solution is independent of Froude numbers at the source and the front and is only a function of time, the drag coefficient, C_D, the volume flux per unit width, q, and the reduced gravity of the intrusion, g'. We note that each of the numerical calculations described above, which have identical values of these parameters, converge to the long-time similarity solution.

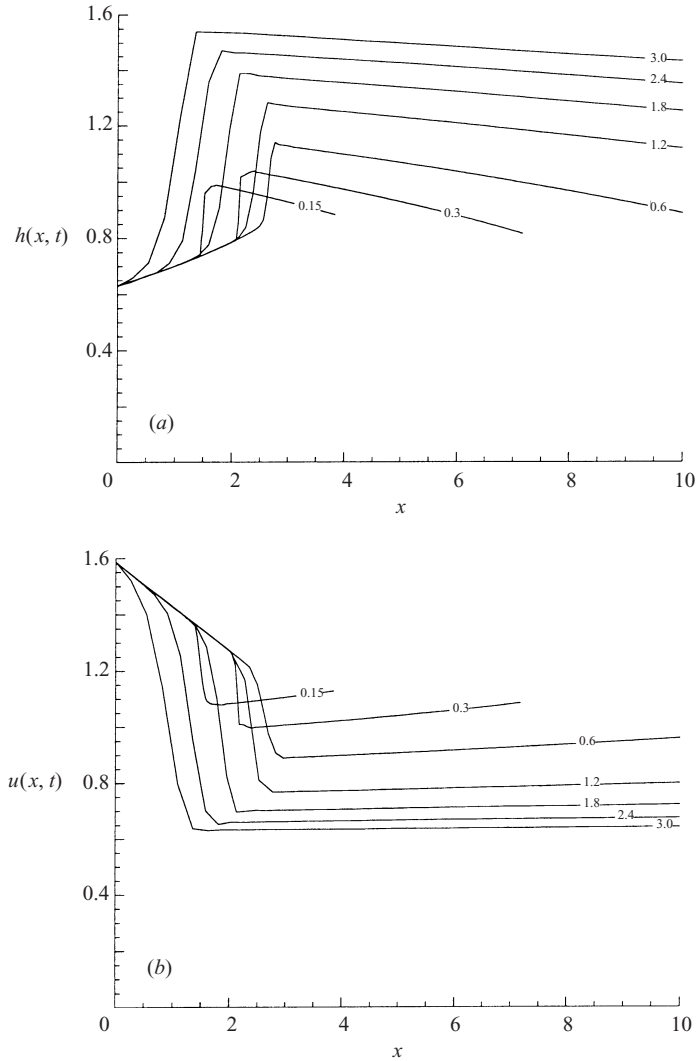

FIGURE 8. The numerically calculated profiles of (*a*) height and (*b*) velocity as functions of distance from the source at various times. These calculations were made with $Fr = 1.2$, $F_0 = 2$ and $C_D = 0.05$. Each profile is labelled with the appropriate value of $C_D t$. Note that the results are displayed only for $0 < x < 10$ in order to illustrate how an internal jump propagates downstream initially but propagates upstream at later times.

6. Particle-driven flows

The analysis and discussion of the preceding sections of this paper have considered the motion of gravity currents which arise from the intrusion of a fluid of one composition into a less dense ambient fluid of a different composition. The density of the intruding fluid has been assumed to exceed that of the overlying ambient owing to compositional differences between the fluids and because the entrainment of the ambient has been neglected, the density of the current remains constant. However, particle-driven gravity currents are also possible (e.g. Bonnecaze *et al.* 1993; Simpson 1997). For these flows, the excess density is due to the suspension of relatively heavy particles. The density of the current is progressively reduced as the particles settle

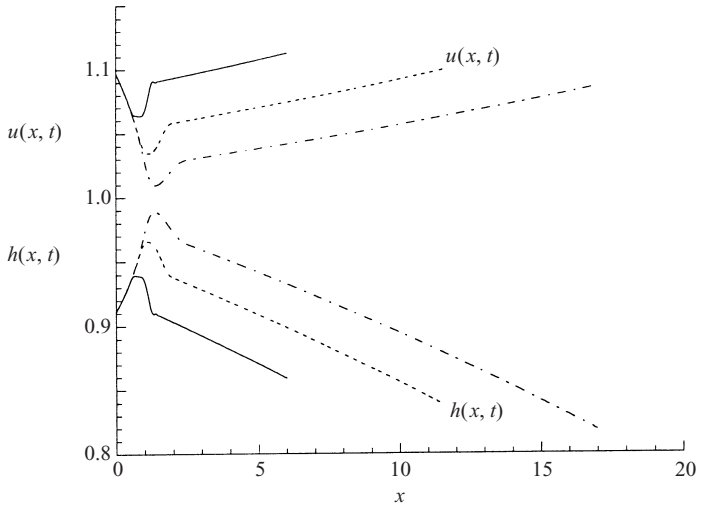

FIGURE 9. The numerically calculated profiles of (*a*) height and (*b*) velocity as functions of distance from the source at times such that $C_D t \ll 1$. These calculations were made with $Fr = 1.2$, $F_0 = 1.15$ and $C_D = 0.01$. The profiles are displayed for ——, $C_D t = 0.05$; - - - - -, 0.10; – · – · –, 0.15.

out of the flow to the underlying boundary. These particle-driven motions have been modelled mathematically using the shallow-water equations in which an expression for the transport and sedimentation of particles is added to those for the conservation of mass and momentum (Bonnecaze *et al.* 1993). In this section, we analyse how basal turbulent drag affects the evolution of such flows.

We denote the volume fraction of particles by ϕ and assume that the excess density of the current over the ambient is due solely to the presence of the suspended particles. Hence

$$\rho_c = \rho_a + \phi(\rho_p - \rho_a), \tag{6.1}$$

where ρ_p is the density of the particulate phase. The initial volume fraction is denoted by ϕ_0 and the scaled volume fraction, ϕ/ϕ_0 is denoted by ψ. In what follows, we analyse the motion of particle-driven gravity currents in a planar geometry ($n = 0$) which arise from the intrusion of a constant flux of particle-laden fluid ($\alpha = 1$). The height and velocity of the current are non-dimensionalized with respect to $(q^2/g')^{1/3}$ and $(qg')^{1/3}$ where the reduced gravity is $g' \equiv g(\rho_p - \rho_a)\phi_0/\rho_a$. In the regime of a dilute suspension $\phi_0 \ll 1$, the expression of the conservation of fluid mass is given by

$$\frac{\partial h}{\partial t} + \frac{\partial}{\partial x}(uh) = 0. \tag{6.2}$$

The momentum equation is now driven by the pressure gradient associated with the suspension of particles and may be written as

$$\frac{\partial}{\partial t}(uh) + \frac{\partial}{\partial x}(u^2 h + \tfrac{1}{2}\psi h^2) = -C_D u^2. \tag{6.3}$$

Finally, on the assumption that the particles are well-mixed throughout the flowing layer and are not resuspended having been deposited to the underlying boundary, the transport and sedimentation of particles is given by

$$\frac{\partial}{\partial t}(h\psi) + \frac{\partial}{\partial x}(hu\psi) = -v_s\psi, \tag{6.4}$$

where v_s is the dimensionless settling velocity of the particles (Bonnecaze *et al.* 1993). The Froude-number condition at the front of the current is now given by

$$u = Fr\sqrt{\psi h} \quad \text{at} \quad x = x_N(t). \tag{6.5}$$

6.1. *Spatially developing flows*

We seek steady-state solutions of these equations on the assumption that the front of the current has travelled sufficiently far downstream that it does not influence the flow. Such solutions, in the absence of drag, have been discussed recently by Bursik & Woods (1996) in the context of sedimenting, volcanic ash-flows and their interaction with topography. Since the flow is generated by a constant flux of particle-laden fluid, the steady-state distribution of the volume fraction of particles is given by

$$\psi = \exp(-v_s x), \tag{6.6}$$

whereas the momentum and mass conservation equations yield

$$\frac{\mathrm{d}}{\mathrm{d}x}(\log u) = \frac{-v_s(\gamma u^4 - \psi)}{2(u^3 - \psi)}, \tag{6.7}$$

where $\gamma = 2C_D/v_s$. The nature of the solution depends upon the magnitude of γ which measures the relative magnitudes of the drag force and the pressure gradient associated with the progressively evolving density of the current. In figures 10(a) and 10(b), we sketch typical solutions for the cases of $\gamma < 1$ and $\gamma > 1$. We note that (6.7) admits two asymptotic solutions for the velocity when $x \gg 1$. These are $u \sim 2/(\gamma v_s x)$ and $u \sim \exp(-v_s x/2)$. To which solution the velocity tends is determined by its initial value and the magnitude of γ.

The 'critical' velocity of these flows which occurs when the local fluid velocity is equal to the speed of propagation of surface waves of long wavelength is given by $u = \sqrt{\psi h}$. Since the volume fraction of particles decays with distance from the source as particles settle to the underlying boundary, the critical velocity also decays. In figures 10(a) and 10(b), we plot the curve which gives the critical velocity, $u = \exp(-\frac{1}{3}v_s x)$. The parameter γ measures the relative importance of the change in fluid velocity due to drag relative to that due to sedimentation. In figures 10(a) and 10(b), we have also plotted the curve $u = \gamma^{-1/4}\exp(-\frac{1}{4}v_s x)$ which corresponds to the condition when the two are equal. The structure of the steady solution is then determined by the magnitude of γ.

For $\gamma < 1$, the effects of sedimentation are of greater significance than the effects of drag and continuous solutions are possible for all initial conditions (figure 10a). Flows which are supercritical at the source ($u(0) > 1$) remain supercritical and tend to $u \sim 2/(\gamma v_s x)$ for $x \gg 1$. Conversely, those which are subcritical ($u(0) < 1$) remain subcritical and tend to $u \sim \exp(-\frac{1}{2}v_s x)$ for $x \gg 1$.

When $\gamma > 1$, the effects of drag exceed those of sedimentation and the structure of these steady-state solutions are different (figure 10b). For a range of initial conditions, the evolution of these spatially developing flows leads to 'hydraulic' catastrophe in which the flow attains the critical velocity. The trajectories of the solutions converge to the curve $u^3 = \psi$ and thereafter continuous, steady solutions are not possible. The precise range of initial conditions leading to this state depends upon the magnitude of γ. The curve $\mathscr{C}_r$ indicates the division between these types of initial conditions. We calculate $\mathscr{C}_r$ by integrating (6.7) from the point at which $\gamma u^4 = \psi$ and $u^3 = \psi$

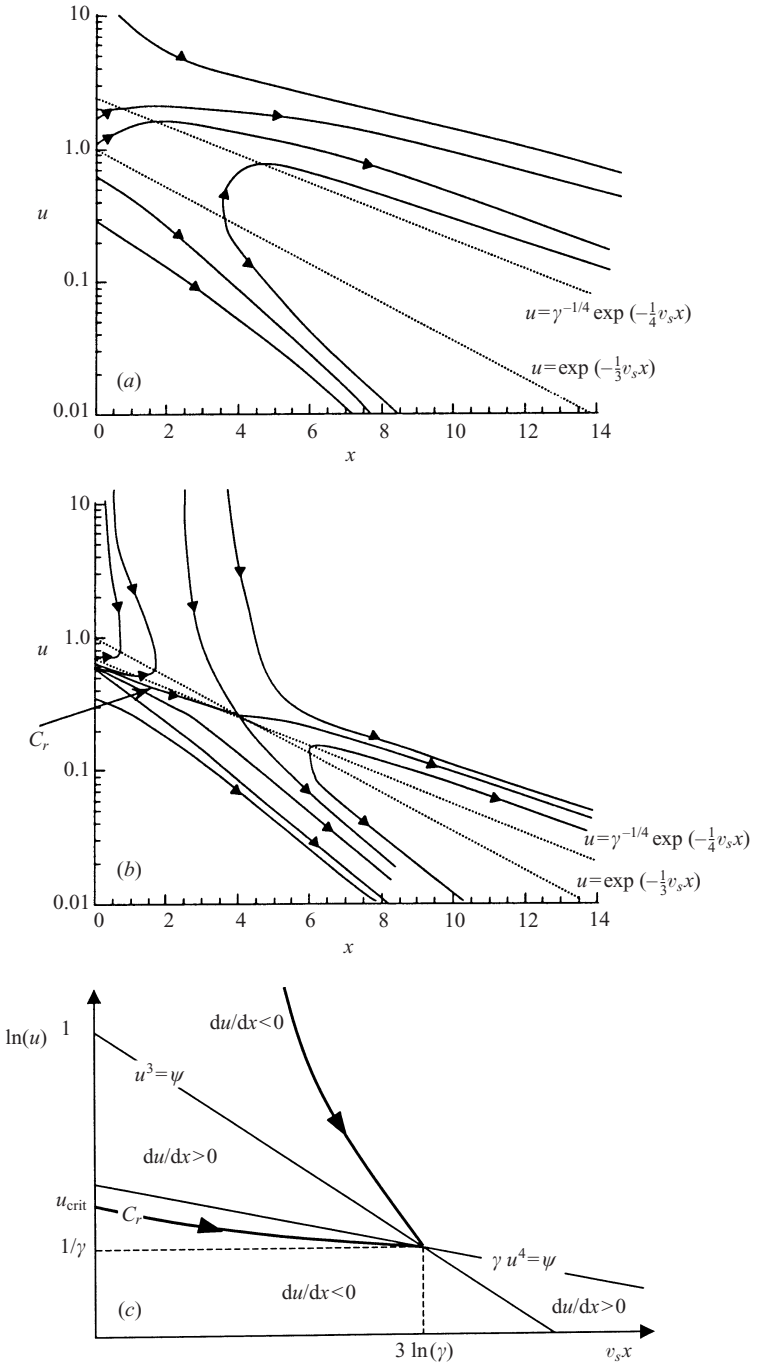

FIGURE 10. Sketch of the trajectories of the solutions for the velocity, $u(x)$ for (a) $\gamma < 1$; (b, c) $\gamma > 1$.

intersect, namely $v_s x = 3\ln\gamma$, back to $x = 0$. When $|v_s x - 3\ln\gamma| \ll 1$ we find

$$u_{\pm} = \frac{1}{\gamma} + \frac{1}{\gamma}\left(-\frac{1}{2} \pm \frac{\sqrt{3}}{6}\right)(v_s x - 3\ln\gamma) + O((v_s x - 3\ln\gamma)^2). \tag{6.8}$$

These expressions provide the expansions for the velocity field, $u(x)$ where the trajectories intersect the point $v_s x = 3\ln\gamma$ and $u = 1/\gamma$. In figure 10(*c*), we plot $\log(u(x))$ as a function of x and from (6.7) indicate the sign of $\mathrm{d}u/\mathrm{d}x$. The curve $\mathscr{C}_r$ runs from $x = 0$ to $u = u_{\rm crit}$ to $v_s x = 3\ln\gamma$, $u = 1/\gamma$ and its expansion in the locality of $v_s x = 3\ln\gamma$ is given by u_- (6.8). The curve $\mathscr{C}_r$, close to this point, is given by u_- (see figure 10*c*). The condition on the initial value of $u(x)$ so that the steady solution is continuous is $u(0) < u_{\rm crit}$. (For example, when $\gamma = 4$, we calculate $u_{\rm crit} = 0.62$.) Discontinuous solutions may arise when $u(0) > u_{crit}$ and these flows undergo a transition from super- to subcritical conditions.

6.2. *Unsteady flows*

In this section, the results of numerical integration of the time-dependent shallow-water equations (6.1)–(6.4) are presented to study the way in which the steady states of § 6.1 may be attained. The numerical method is identical to that of § 5, although the run times are slightly increased as there are now three dependent variables, namely u, h and ψ. We present two sets of results. In the first, the Froude number at the source and front are equal to 1.2, and $\gamma = 0.4$. We note that the flow evolves towards a continuous steady state (figure 11). In this regime, the effects of sedimentation are to reduce the critical velocity more rapidly than the rate of decrease of the flow speed. Thus, the flow always remains supercritical and evolves smoothly towards a continuous steady state.

For the second set of results, we impose both Froude numbers equal to 1.2 while $\gamma = 4$ (figure 12). These flows lead to the 'hydraulic' catastrophe described above (§ 6.1). Thereafter the flows evolve in an unsteady and discontinuous manner. A backward propagating bore is initiated from the downstream location at which the velocity has first become critical. This corresponds to the point at which $u^3 = \psi$. The bore propagates towards the source with a diminishing velocity. It may become stationary if there is sufficient energy within the initial flow to account for that required by the subcritical flow to which the transition occurs and for that dissipated by the internal jump. In the example shown this is not so, and a bore propagates all the way back to the source. Conversely, if there is sufficient energy in the flow, then a stationary jump is attained.

7. Conclusions and applications

The models presented herein illustrate the role of bottom friction in modifying the propagation of a turbulent gravity current over a horizontal plane. The effects become important at long times and we have studied in detail the development of a flow from a steady source. The initial phase of the motion is governed by an inertia–buoyancy balance, as described by Gratton & Vigo (1994), but, at later times, the dynamics are controlled by a balance between buoyancy and drag forces. The models illustrate that the transition occurs at the front of the current, which adjusts to a more gradual spreading regime. The fluid behind the nose therefore builds up and a backward-propagating adjustment wave develops.

It is of interest to examine conditions under which the bottom friction may be important in two geophysical examples. We consider a dense turbidity current, in which the subaqueous flow is driven by particles (Sparks *et al.* 1993) and volcanic ash flows in which the subaerial flow is again driven by the presence of dense particles (Bursik & Woods 1996). In both cases, the key issue in determining the control of the dynamics is the rate at which sedimentation of dense, suspended particles reduces

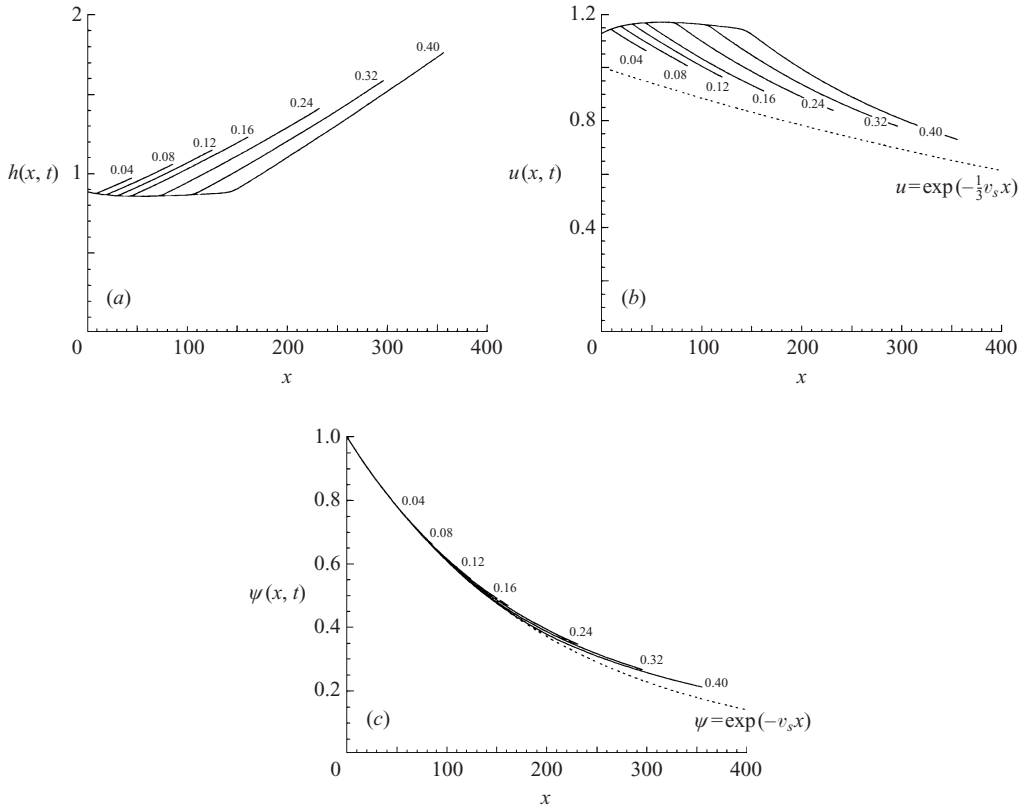

FIGURE 11. The numerically calculated profiles of (*a*) height, (*b*) velocity and (*c*) volume fraction of particles as functions of distance from the source at various times. These calculations were made with $Fr = 1.2$, $F_0 = 1.2$, $C_D = 0.001$ and $v_s = 0.005$. Each profile is labelled with the appropriate value of t. Note that in this calculation $\gamma < 1$ and the flows evolve downstream continuously towards the steady state. (*b*) - - - - -, 'critical' velocity; (*c*) - - - - -, the steady-state for ψ.

the buoyancy compared to the magnitude of the drag force. The relative importance of these two effects and the time scales over which they become non-negligible is measured by the magnitude of the parameter γ, which may be explained as follows. The dimensional timescale on which drag forces significantly influence the flow is given by $t_d \sim C_D^{-1}(q/g'^2)^{1/3}$ (see §§ 2 and 3). The length scale over significant sedimentation occurs scales as q/V_s, where V_s is the dimensional settling velocity of the suspended particles. Hence, the timescale is given by $t_s \sim (qg')^{-1/3}\, q/V_s$. Thus, the ratio of these two time scales $t_s/t_d \sim C_D(qg')^{1/3}/V_s$ is equivalent to the parameter γ (see § 6). The dynamics of the flow are dominated by sedimentation if $\gamma \ll 1$, whereas drag effects are more important if $\gamma \gg 1$.

For many geophysical flows, the drag coefficient, C_D, is estimated to be in the range 10^{-2}–10^{-3} (Parker, Fukushima & Pantin 1986), while the initial reduced gravity, g' is in the range 10^{-1}–$10\,\mathrm{m\,s^{-2}}$. In turbidities, the fall speed of particles of typical size 1–100 μm lies in the range 10^{-4}–$10^{-2}\,\mathrm{m\,s^{-1}}$, whereas in ash flows, the typical fall speed of particles is of order 10^{-1}–$1\,\mathrm{m\,s^{-1}}$. We may thus estimate the magnitudes of flow which become strongly influenced by bottom friction before most of the sedimentation has occurred.

For a channelled ash flow, sedimentation will dominate the effects of turbulent drag in flows with volume fluxes smaller than about $10^3\,\mathrm{m^2\,s^{-1}}$. Thus, only in the

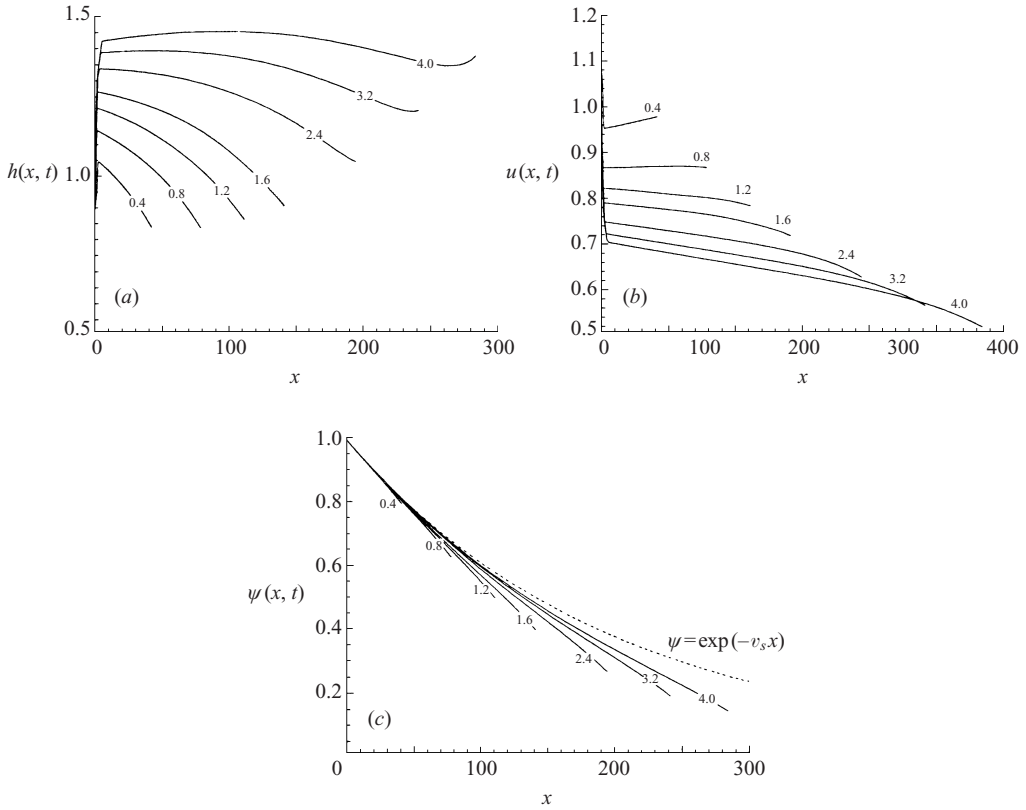

FIGURE 12. The numerically calculated profiles of (*a*) height, (*b*) velocity and (*c*) volume fraction of particles as functions of distance from the source at various times. These calculations were made with $Fr = 1.2$, $F_0 = 1.2$, $C_D = 0.01$ and $v_s = 0.005$. Each profile is labelled with the appropriate value of t. Note that in this calculation $\gamma > 1$ and the flows evolves to the steady state by means of an internal jump, which is established by a backward propagating bore from the location at which the flow first attains critical conditions. (*c*) - - - - -, steady-state for ψ.

most extreme eruptions is the turbulent drag likely to influence the flow. By contrast, however, in long-lived turbidities with typical volume fluxes of order $10\,\mathrm{m}^2\,\mathrm{s}^{-1}$, the effects of drag are likely to become important long before substantial sedimentation has occurred. As we have seen in the calculations of this paper, this will limit the range of propagation and the sedimentation profile of the current relative to the predictions of models invoking a buoyancy–inertial balance. The propagation speeds are significantly reduced and the suspended sediment is deposited closer to the source.

In closing, we note that it would also be interesting to develop some of the present ideas to account for the effects of a sloping boundary and for the effects of mixing of ambient fluid with the effect of the current.

A. J. H. acknowledges the financial support of the EPSRC.

Appendix A

In this Appendix, we generalize the new similarity solution of § 4, in which the basal drag is in balance with a streamwise pressure gradient, to include axisymmetric geometry and a variable source, given by (2.4). In terms of dimensional variables

for which x_N is the distance from a line source or a point source in planar or axisymmetric geometry, respectively, the balance between the drag and the pressure gradient implies

$$g'h/x_N \sim C_D u^2/h. \tag{A 1}$$

The global expression for the conservation of mass yields

$$x_N^{n+1}\, h \sim q t^{\alpha}, \tag{A 2}$$

where $n = 0$ for planar geometry and $n = 1$ for axisymmetric geometry. Finally, for kinematic consistency we require $u \sim x_N/t$. Therefore, we seek a similarity solution of the form

$$x_N = X_0[C_D g' q^2\, t^{(2\alpha+2)}]^{1/(2n+5)}, \tag{A 3}$$

$$u = \frac{2\alpha+2}{2n+5} X_0[C_D g' q^2\, t^{(2\alpha-2n-3)}]^{1/(2n+5)}\, \mathscr{U}(\xi), \tag{A 4}$$

$$h = \frac{2\alpha+2}{2n+5} X_0^{3/2}\, [C_D^{-(n+1)}\, q^3\, g'^{-(n+1)}\, t^{(3\alpha-2n-2)}]^{1/(2n+5)}\, \mathscr{H}(\xi), \tag{A 5}$$

where the similarity variable is given by $\xi = x/x_N$. Substitution of these expressions into the equation for the conservation of mass yields

$$(3\alpha - 2n - 2)\mathscr{H} - (2\alpha+2)\xi \frac{\mathrm{d}\mathscr{H}}{\mathrm{d}\xi} + \frac{2\alpha+2}{\xi^n} \frac{\mathrm{d}}{\mathrm{d}\xi}(\xi^n\, \mathscr{U}\mathscr{H}) = 0. \tag{A 6}$$

The dominant terms in the momentum equation at long times depends upon the magnitude of α. Provided that $\alpha < 4$, we find that, for $t \gg 1$, the momentum equation is given by

$$\frac{\mathrm{d}\mathscr{H}}{\mathrm{d}\xi} = -\frac{\mathscr{U}^2}{\mathscr{H}}. \tag{A 7}$$

The boundary conditions at the front of the current are given by

$$\mathscr{H}(1) = 0, \quad \mathscr{U}(1) = 1. \tag{A 8}$$

The global conservation of mass is now given by

$$\frac{2\alpha+2}{2n+5} X_0^{(2n+5)/2} \int_0^1 \xi^n\, \mathscr{H}\, \mathrm{d}\xi = 1. \tag{A 9}$$

This system of ordinary differential equations and boundary conditions could be integrated to determine the profiles within the current. In what follows, we consider only the cases of flows generated by the instantaneous release of dense fluid ($\alpha = 0$).

Constant volume gravity currents ($\alpha = 0$)

For this case, the equations admit exact similarity solutions. They are given by

$$\mathscr{U} = \xi, \tag{A 10}$$

$$\mathscr{H} = (\tfrac{2}{3})^{1/2}(1 - \xi^3)^{1/2}. \tag{A 11}$$

The constant, X_0, is evaluated by substitution into (A 9). For two-dimensional flows ($n = 0$), $X_0 = 1.68$ and for axisymmetric flows ($n = 1$), $X_0 = 2.01$.

REFERENCES

Benjamin, T. B. 1968. Gravity currents and related phenomena. *J. Fluid Mech.* **88**, 223–240.

Bonnecaze, R. T., Huppert, H. E. & Lister, J. R. 1993 Particle-driven gravity currents. *J. Fluid Mech.* **250**, 339–369.

Bursik, M. & Woods, A. W. 1996 The dynamics and thermodynamics of ash flows. *Bull. Volcanol.* **58**, 175–193.

Dressler, R. F. 1952 *J. Res. Natl Bur. Stand.* **49**, 217.

Gratton, J. & Vigo, C. 1994 Self-similar gravity currents with variable inflow revisited: plane currents. *J. Fluid Mech.* **258**, 77–104.

Grundy, R. E. & Rottman, J. W. 1986 Self-similar solutions of the shallow-water equations representing gravity currents with variable inflow. *J. Fluid Mech.* **169**, 337–351.

Hallworth, M. A., Huppert, H. E., Phillips, J. C. & Sparks, R. S. J. 1996 Entrainment into two-dimensional and axisymmetric turbulent gravity currents. *J. Fluid Mech.* **308**, 289–312.

Hatcher, L., Hogg, A. J. & Woods, A. W. 2000 The effects of drag on turbulent gravity currents. *J. Fluid Mech.* **416**, 297–314.

Hogg, A. J., Ungarish, M. & Huppert, H. E. 2000 Particle gravity currents: asymptotic solutions and box models. *European J. Mech.* B **19**, 139–165.

Hoult, D. P. 1972 Oil spreading on the sea. *Annu. Rev. Fluid Mech.* **2**, 341–368.

Huppert, H. E. 1982 The propagation of two-dimensional and axisymmetric viscous gravity currents over a rigid horizontal surface. *J. Fluid Mech.* **121**, 43–58.

Huppert, H. E. & Simpson, J. E. 1980 The slumping of gravity currents. *J. Fluid Mech.* **99**, 785–799.

Huppert, H. E. & Woods, A. W. 1995 Gravity-driven flows in porous layers. *J. Fluid Mech.* **292**, 557–594.

Moody, L. F. 1944 Friction factors for pipe flows. *Trans. ASME* **66**, 671.

Parker, G., Fukushima, Y. & Pantin, H. 1986 Self-accelerating turbidity currents. *J. Fluid Mech.* **171**, 145–181.

Sherman, F. S., Imberger, J. & Corcos, G. M. 1978 Turbulence and mixing in stably stratified waters. *Annu. Rev. Fluid Mech.* **10**, 267–288.

Simpson, J. E. & Britter, R. E. 1979 The dynamics of the head of a gravity current advancing over a horizontal surface. *J. Fluid Mech.* **94**, 477–495

Simpson, J. E. 1997 *Gravity Currents in the Environment and the Laboratory*. Cambridge University Press.

Sparks, R. S. J., Bonnecaze, R. T., Huppert, H. E., Lister, J. R., Hallworth, M. A., Mader, H. & Phillips, J. C. 1993 Sediment-laden gravity currents with reversing buoyancy. *Earth Planet. Sci. Lett.* **114**, 243–257.

Turner, J. S. 1973 *Buoyancy Effects in Fluids*. Cambridge University Press.

Ungarish, M. & Huppert, H. E. 1998 The effects of rotation on axisymmetric gravity currents. *J. Fluid Mech.* **362**, 17–51.

Whitham, G. B. 1955 Effects of hydraulic resistance in the dam-break problem. *Proc. R. Soc. Lond.* **227**, 399–407.

Whitham, G. B. 1973 *Linear and Non-linear Waves*. Wiley.

Wilkinson, D. L. & Wood, I. R. 1971 A rapidly varied flow phenomenon in a two layer flow. *J. Fluid Mech.* **47**, 241–256.

Yih, C. S. & Guha, C. R. 1955 Hydraulic jumps in a fluid system of two layers. *Tellus* **7**, 358–366.